Identification of potent and selective small molecule inhibitors of the cation channel TRPM4

Lijo Cherian Ozhathil*[1], Clémence Delalande*[2], Beatrice Bianchi[1], Gabor Nemeth[2], Sven Kappel[1], Urs Thomet[1], Daniela Ross-Kaschitza[1], Céline Simonin[2], Matthias Rubin[1], Jürg Gertsch[1], Martin Lochner[1,2], Christine Peinelt[1], Jean-Louis Reymond[2], Hugues Abriel[1]

Running Title: Potent TRPM4 inhibitors

Affiliations:

1: Institute of Biochemistry and Molecular Medicine, National Center of Competence in Research NCCR TransCure, University of Bern, Bühlstrasse 28, 3012 Bern (Switzerland)

2: Department of Chemistry and Biochemistry, National Center of Competence in Research NCCR TransCure, University of Bern, Freiestrasse 3, 3012 Bern (Switzerland)

*** Co-first authors.**

Corresponding authors:

Hugues Abriel
Institute of Biochemistry
and Molecular Medicine
National Center of Competence in Research
NCCR TransCure
University of Bern, Bühlstrasse 28, 3012 Bern
(Switzerland)
E-mail: hugues.abriel@ibmm.unibe.ch

Jean-Louis Reymond
Department of Chemistry and Biochemistry
National Center of Competence in Research
NCCR TransCure
University of Bern, Freiestrasse 3, 3012 Bern
(Switzerland)
E-mail: jean-louis.reymond@dcb.unibe.ch

Acknowledgements:

We thank Jean-Sebastien Rougier, PhD and Sarah Vermij for helpful discussions and critical proof reading. This work was supported by NCCR Transcure 51NF40-160620 and a grant by the Swiss Heart Foundation to Hugues Abriel.

BACKGROUND AND PURPOSE

TRPM4 is a calcium-activated nonselective cation channel expressed in many tissues and implicated in several diseases, and has not yet been validated as a therapeutic target due to the lack of potent and selective inhibitors. We sought to discover a novel series of small-molecule inhibitor by combining *in silico* methods and cell based screening assay, with sub-micromolar potency and improved selectivity from previously reported TRPM4 inhibitors.

EXPERIMENTAL APPROACH

Here, we developed a HTS compatible assay to record TRPM4-mediated Na^+ influx in cells using a Na^+-sensitive dye and used this assay to screen a small set of compounds selected by ligand-based virtual screening using previously known weakly active and non-selective TRPM4 inhibitors as seed molecules. Conventional electrophysiological methods were used to validate the potency and selectivity of the hit compounds in HEK293 cells overexpressing TRPM4 and in endogenously expressing prostate cancer cell line LNCaP. Chemical chaperone property of compound **5** was studied using western blots and electrophysiology experiments.

KEY RESULTS

A series of halogenated anthranilic amides were identified with TRPM4 inhibitory properties with sub-micromolar potency and adequate selectivity. We also show for the first time that a naturally occurring variant of TRPM4, which display loss-of-expression and function, is rescued by the most promising compound **5** identified in this study.

CONCLUSIONS AND IMPLICATIONS

The discovery of compound **5**, the most potent and selective inhibitor of TRPM4 with an additional chemical chaperone feature, revealed new opportunities for studying the role of TRPM4 in human diseases and developing clinical drug candidates.

KEYWORDS:

TRP channels, TRPM4, drug discovery, ligand based virtual screening, 9-phenanthrol, chemical chaperone, prostate cancer.

ABBREVIATIONS:

TRPM4

Transient receptor potential cation channel subfamily M member 4

HTS

High throughput screening

HEK 293

Human embryonic kidney cells 293

LNCaP

Lymph node carcinoma of the prostate

INTRODUCTION

The ion channel TRPM4 belongs to the 28-member TRP (transient receptor potential) channel family. It is activated upon increase of intracellular Ca^{2+} and conducts monovalent cations such as Na^{+}, K^{+}, and Cs^{+}, hence modulating the transmembrane electrical potential. TRPM4 is expressed in many cell types and tissues, but its role in physiology is still poorly understood (Launay et al., 2002; Nilius et al., 2003; Fonfria et al., 2006). With regard to its role in human diseases, more than 20 *TRPM4* genetic variants have been described in families with cardiac conduction alterations such as

progressive conduction block and congenital atrioventricular block (AVB) (Kruse and Pongs, 2014; Syam et al., 2016). A significant number of these pathogenic TRPM4 variants leads to gain-of-expression and function, while others to loss-of-expression and function (Kruse et al., 2009; Liu et al., 2010, 2013; Syam et al., 2016). Based on studies with experimental autoimmune encephalitis (EAE) mice model, TRPM4 has been suggested to be a key player in the neurodegenerative process of multiple sclerosis (Schattling et al., 2012; Malhotra et al., 2013; Makar et al., 2015). Interestingly TRPM4-deficient mice with EAE displayed much milder clinical manifestations than wild-type (WT) EAE mice (Schattling et al., 2012). Recently, TRPM4 has also been shown to be involved in migration and proliferation of human prostate cancer cells (Ashida et al., 2004; Singh et al., 2006; Suguro et al., 2006; Prevarskaya et al., 2007; Schinke et al., 2014; Holzmann et al., 2015; Berg et al., 2016; Sagredo et al., 2017). Taken together, these recent findings strongly suggest that TRPM4 is a potential pharmacological target for treating neurological and cardiovascular disorders, as well as certain types of cancer.

Most of the characterizations of TRPM4 in different tissues have heavily relied on patch clamp technique with pharmacological inhibitors that have several issues. Until now, 9-phenanthrol has been the most commonly used TRPM4 inhibitor to dissect its roles in physiology and diseases (***Figure 1***) (Grand et al., 2008; Guinamard et al., 2014). However, the low potency and lack of selectivity of 9-phenanthrol on TRPM4 limit its usefulness in studies using animal models or primary cell lines (Burris et al., 2015; Garland et al., 2015). Other reported TRPM4 inhibitors include flufenamic acid (FFA), (***Figure 1***) acting similarly weakly on TRPM4 but with a longer list of documented off-target effects that are related to its primary role as a non-steroidal anti-inflammatory drug (Gardam et al., 2008). While glibenclamide, an even weaker TRPM4 inhibitor also inhibit ATP-dependent K^+ channel, which are its primary targets in treatment of type II diabetes (Demion et al., 2007; Alexander et al., 2013).

Here, we developed a fluorescence cell-based screening assay monitoring TRPM4-induced Na^+ influx using an intracellular Na^+ specific dye (Asante Natrium Green-II, ANG-II). This assay allowed reliable assessment of TRPM4 activity modulation by small molecules. In the absence of structural

information on inhibitor binding sites on TRPM4, we used a ligand-based virtual screening (LBVS) approach (Scior et al., 2012) to search commercially available compounds for analogs of the above mentioned weak and non-selective TRPM4 inhibitors (Sterling and Irwin, 2015). We performed LBVS with the 3D-shape and pharmacophore similarity algorithm xLOS (atom category eXtended Ligand Overlap Score) as similarity measure. xLOS is a scaffold-hopping algorithm (Schneider et al., 1999) that recently proved its validity in related searches for selective Ca^{2+} channel (Simonin et al., 2015) and kinase inhibitors (Kilchmann et al., 2016). Activity screening of a small series of compounds selected by LBVS procedure allowed us to rapidly identify anthranilic amides **4** and **5**, two analogs of FFA with a 10-fold stronger and more selective inhibition of TRPM4 compared to 9-phenanthrol (***Figure 1***). Structure-activity relationship (SAR) study further uncovered **6** as the first selective sub-micromolar TRPM4 inhibitor. These TRPM4 blockers reversibly inhibit the overexpressed TRPM4 channels in HEK293 cells and block TRPM4-mediated currents in human prostate cancer cells. Their direct and specific interaction with TRPM4 is further exemplified by their activity as chemical chaperone to rescue the expression and activity of a loss-of-function TRPM4 variant. These results prepare the way for more potent and specific TRPM4 inhibitors.

RESULTS

Development and validation of a TRPM4 dependent Na^+ influx-screening assay

First, we developed a Na^+ influx assay to screen large libraries of chemically diverse small molecules. We used a cell line stably expressing TRPM4 under a tetracycline-inducible promoter (Amarouch et al., 2013). Functional membrane expression of TRPM4 in the tetracycline-induced cells was compared with the non-induced cells and non-transfected HEK293 cells. Furthermore, endogenous expression of TRPM4 in HEK293 cells as reported in our previous studies (Amarouch et al., 2013) was knocked down by CRISPR/Cas9 technology (KD) (***Figure 2A and Supporting information***

Figure S1). In order to perform FLIPR (Fluorescent Imaging Plate Reader) based screening of compounds, the cells were pre-incubated with Na^+-free assay buffer to deplete intracellular Na^+, followed by loading the cells with a Na^+-sensitive ANG-II dye. Reintroducing Na^+ along with ionomycin in the stimulus buffer for Ca^{2+}-dependent activation of TRPM4 resulted in an increase of fluorescence signal over the baseline **(*Figure 2B*)**. We used the area under the curve (AUC) **(*marked area, Figure 2B*)** to quantify the signal intensity with or without ionomycin. Upon TRPM4 overexpression, the fluorescence signal increased three fold compared with non-transfected HEK293 or KD cells **(*Figure 2B*)**. The increase in fluorescence in non-transfected HEK293 cells and non-induced TRPM4 cells could be due to Na^+ influx via various endogenous Na^+ transporters **(*Figure 2B*);** however, the effect is significantly smaller than in TRPM4-overexpressing cells ***(Figure 2B).*** Following the demonstration that the ANG-II dye could detect Na^+ influx, which was largely mediated through TRPM4 channel activation, we further assessed the dependence of the fluorescence signal on the extracellular Na^+ and Ca^{2+} concentration in the stimulus buffer. We determined Na^+ dependence with stimulus buffer containing different concentrations of Na^+ by replacing the ion with equimolar N-methyl-d-glucamine (NMDG). ANG-II dye presented an affinity for Na^+ ions with a Michaelis-Menten constant K_m of 76.6 ± 6.3 mM ***(Figure 2C).*** Next, we determined Ca^{2+} dependence using stimulus buffer containing 140 mM Na^+ and varying concentrations of extracellular Ca^{2+} without any chelator. The increase in fluorescence signal showed a dependence on Ca^{2+} concentration in the stimulus buffer with an EC_{50} of 0.2 ± 0.1 mM ***(Figure 2D).*** We finally assessed the robustness of the assay by monitoring the statistical Z` factor, which always scored 0.5 or more in all our experiments, while the ratio of AUC in presence and absence of ionomycin remained above 2 **(*Supporting information Figure S2, A and B*)**. Finally, the assay developed here tolerated DMSO up to 1%, the highest concentration used to dissolve the test compounds **(*Supporting information Figure S2, C and D*).**

Discovery of small molecule TRPM4 inhibitors

To identify potent TRPM4 inhibitors, we performed a focused screening campaign using LBVS with xLOS (Simonin et al., 2015) to search a catalog of 900,000 commercially available drug-like small

molecules for analogs of the known but relatively weak TRPM4 inhibitors 9-phenanthrol, FFA and glibenclamide (***Figure 1***). We selected 214 compounds among the top scoring virtual hits, purchased 1 mg solid samples which we conditioned as 10 mM stock solution in DMSO, and screened these compounds for inhibition of TRPM4 at 10 µM using 9-phenanthrol (25 µM) as positive control **(*Figure 3Ai*)**. Initial screen revealed three hits for which we purchased and tested an additional 247 analogs selected by LBVS with xLOS as well as other fingerprint similarity search methods (Awale and Reymond, 2014). As a result of these screening efforts, we identified four hits, compounds **4, 5, 8** and **9**, repurchased 25 mg solid samples, and confirmed their inhibitory activity at 5 µM concentration ***(Figure 1 and Figure 3 Aii)***. These compounds inhibited the initial rate of TRPM4-mediated Na^+ influx in a concentration-dependent manner. The best TRPM4 inhibitors were the aryloxyacyl-anthranilic acids **4** (IC_{50} = 1.6 ± 0.3 µM) and **5** (IC_{50} = 1.5 ± 0.1 µM, ligand efficiency (LE) = 0.371), showing a 20 times stronger inhibition than 9-phenanthrol (IC_{50} = 29.1 ± 5.8 µM) ***(Figure 3B - D).***

Structure-activity relationship (SAR) study of TRPM4 inhibitors

For SAR studies, we initially focused on anthranilic inhibitor **5** and devised a synthetic route for varying substituents on both aromatic rings and within the acetyl linker and prepared 49 analogs. (***Figure 4A***, ***Table 1, and Supporting information Table S1-S3***). Changing the substituents of the aromatic ring often abolished the activity of the compound. However, 13 anthranilic acid derivatives showed TRPM4 inhibition with IC_{50} values in the range 1-10 µM, confirming the robustness of the identified scaffold ***(Table 1, Figure 1)***. Overall the results obtained with the different analogs indicated that TRPM4 inhibition required the presence of the anthranilic acid moiety with a halogen substituent at position 4 and a defined substitution pattern on the aryloxy group ***(Figure 4B)***. The SAR profile uncovered the 1-naphthyloxy analogs **6** as the first submicromolar inhibitor in the series with an IC_{50} = 0.4 ± 0.3 µM (LE = 0.345) (***Table 1***). However, when considering its LE (Hopkins et al., 2014), compound **6** does not bring additional improvement over compound **5.** On the other hand, pure enantiomers (>99% ee) of **4** (**52** and **53**) were obtained using preparative chiral-phase HPLC and analyzed for purity using the same method. Both enantiomers were similarly active and chirality of

the linker did not significantly influence activity,(***Supporting information Table S3***), while other modifications of the linker were detrimental to activity (**54 to 58,** ***Supporting information Table S3***).

Compound 5 selectively inhibits TRPM4 overexpressed in HEK293 cells

To gain further insight into the three most potent inhibitors found here **4**, **5** and **6** , we analyzed their predicted off-target effects using the polypharmacology browser (Awale and Reymond, 2017), an online tool that predicts possible biological activity by multi-fingerprint comparisons with bioactive compounds from the ChEMBL database (Gaulton et al., 2012). While **4** and **5** were essentially free of off-target predictions, we found that **6** had a reported activity at 10 μM on GLPR1 (glucagon-like peptide receptor 1) ***(https://pubchem.ncbi.nlm.nih.gov/bioassay/624417 (accessed July 6, 2017))***.

We further confirmed the inhibitory activity of compounds **4** and **5** using classical patch-clamp electrophysiology recordings on TRPM4 overexpressing cell line. In excised membrane patches, we quantified TRPM4 inhibition using the generic TRPM4 inhibitors 9-phenanthrol **(*Figure 5A*)** and FFA (***Figure 5B***), and compared it with our newly identified hit compounds **4 (*Figure 5C*)** and **5** ***(Figure 5D)***. Maximal current at +100 mV was used to construct concentration-response curves **(Average current traces:** ***Supporting information Figure S3***). Interestingly, both compounds inhibited TRPM4 with an IC_{50} of 1.0 ± 0.2 and 1.8 ± 0.1 μM for **4** and **5** respectively, which are several times more potent than IC_{50} values of 17.0 ± 2.8 and 9.2 ± 1.2 μM for 9-phenanthrol and FFA, respectively. In addition, we also observed reversible inhibition by **4** and **5** when applied to the cytosolic side of the ruptured membrane patches. **(*Supporting information Figure S4*).**

Further, to evaluate the selectivity of the newly identified hits against TRPM5, the closest homolog of TRPM4, we performed excised membrane voltage clamp recordings on HEK293 cells expressing TRPM5. As a positive control, we used triphenylphosphine oxide (TPPO), a known TRPM5 inhibitor at 20 μM. (Palmer et al., 2010). TPPO inhibited TRPM5 current but did not affect TRPM4 current **(*Figure 5Ei and Eii*)**. However, compound **4** had a variable potentiating effect on TRPM5, while compound **5** had no significant effect on the TRPM5 current **(*Figure 5Ei*)**. In addition, we also tested the selectivity of compound **5** against other TRP family members including TRPM7, TRPM8, TRPV1

and TRPV6 using whole-cell patch clamp recordings. At 10 or 100 μM, compound **5** did not show any inhibition of currents from these targets **(*Supporting information Figure S5*)**.

Next we investigated if compound **5** had any off target effects on 17 different ion channel proteins and membrane receptors, including Gamma-aminobutyric acid receptor subunit alpha-1(GABA(A1)), N-methyl-D-aspartate (NMDA) receptor, Ca^{2+} channel and voltage gated K^+ channels, which are targets of the parent drug FFA. At 10 μM compound **5** did not show any significant effect on these targets, and showed only < 5% inhibition of dofetilide binding to the cardiac hERG channel. (***Supporting information Table S4***).

Compound 5 inhibits endogenous TRPM4 currents in LNCaP prostate cancer cells

We next assessed if compound **5** also inhibits endogenous TRPM4 currents. We recorded TRPM4 whole- cell currents with 10 μM Ca^{2+} in the patch pipette in the prostate cancer cell line LNCaP as described previously (Holzmann et al., 2015; Kilch et al., 2016). The currents activated slowly (***Figure 6A*)** with the typical TRPM4 current-voltage relationship (I-V) shown in ***Figure 6B***. After TRPM4 currents were activated, we applied compound **5** at different concentrations. Compound **5** inhibited TRPM4 currents reversibly in a concentration dependent manner with an IC_{50} of 1.1 ± 0.3 μM (***Figure 6C***). This is consistent with our findings in a TRPM4 overexpression system (***Figure 3 and 5***), where compound **5** also inhibits TRPM4 currents with an IC_{50} of~1 μM.

Compound 5 rescues functional expression of A432T, a loss-of-expression TRPM4 variant

Based on the TRPM4 selectivity of compound **5**, we investigated whether compound **5** can rescue membrane expression of TRPM4 A432T, a loss-of-expression variant found in cardiac AVB patients (Syam et al., 2016). It is reported that decreased expression and altered trafficking of ion channel disease causing variants, such as in CFTR and hERG, can be corrected either by incubation at a lower temperature or by using selective chemical compounds (Denning et al., 1992; Zhou et al., 1999). We followed a similar strategy and observed that the expression of A432T was increased after a 24-hour long incubation of the cells at 28 °C **(*Supporting information Figure S6 A*)**.

Next we pre-incubated cells expressing A432T with 50 µM compound **5** overnight and evaluated any change in A432T total and surface expression using western blot (***Figure 7Ai***). Compound **5** showed only~ 30% cytotoxicity at 100 µM, making it feasible for longer incubation with cells (***Supporting information Figure S7***). Densitometric quantification of the upper fully glycosylated (FG) and the lower core glycosylated (CG) bands showed partial rescue of total and surface expression(biotinylated fraction) of A432T by compound **5 (*Figure 7Aii*) .** We further evaluated if the rescued expression of A432T with pre-incubation of compound **5** also led to increase in current density in excised membrane patches. As illustrated in ***Figure 7 B and C***, A432T showed a significant decrease in the Ca^{2+} sensitive outward current in comparison to WT. Pre-incubation with compound **5** at 50 µM overnight and followed by a washout before current recordings, partially rescued the functional expression and the Ca^{2+} sensitive outward current of A432T. Conversely, an inactive congener of compound **5**, i.e. compound **51**, did not rescue the expression of A432T at 50 µM **(*Figure 7D*)**.

Selectivity of compound **5** for rescuing A432T was further evaluated by incubating the loss-of-expression hERG variant named Dupl hERG, which was found in a congenital long-QT syndrome patient (Grilo et al., 2010), both with 50 µM compound **5** and with lower-temperature (28 °C) incubation. As presented in (***Supporting information Figure S6 B*)**, Western blot experiments showed that a reduction of incubation temperature rescued the trafficking defect of Dupl hERG, whereas no effect was observed after incubation with compound **5**. However, the rescuing property of compound **5** was not limited to A432T but also increased WT TRPM4 expression similar to incubation with lower temperature **(*Supporting information Figure S6 C and D)*** .

DISCUSSION AND CONCLUSION

Human mutations in the TRPM4 gene have been implicated in cardiac conduction disorders (Kruse et al., 2009; Liu et al., 2010, 2013; Stallmeyer et al., 2012; Syam et al., 2016). So exploring the role of TRPM4 in cardiac physiology and pathophysiology upholds great clinical relevance. However, most of these physiological characterizations relied upon patch clamp studies with TRPM4 KO mice models combined with pharmacological inhibitors. Notably, the most reported TRPM4 inhibitor, 9-

phenanthrol, did show some selectivity for TRPM4 compared to other TRP channels. However, it is not sufficiently potent, and high concentrations reversibly inhibit delayed outward rectifying K^+ and voltage-gated Ca^{2+} currents in mouse ventricular myocytes (Simard et al., 2012). A recent study showed that 9-phenanthrol inhibits TMEM16A, a Ca^{2+}-activated Cl^- channel in arterial smooth myocytes (Burris et al., 2015). Furthermore, 9-phenanthrol belongs to the class of polycyclic aromatic hydrocarbons, which contribute to its cellular toxicity (Feng et al., 2012). The non-steroidal anti-inflammatory drug FFA and glibenclamide are also used as TRPM4 inhibitors (Ullrich et al., 2005; Demion et al., 2007). Although these compounds inhibit TRPM4 current reversibly, they also have many off target effects on other ion channels (Gardam et al., 2008; Alexander et al., 2013). These findings support the need for more potent and selective TRPM4 inhibitors. In this study, we developed a novel Na^+-sensitive screening assay and performed a focused screening campaign using LBVS with xLOS, which lead to the identification of compounds **4**, **5** and **6,** as potent TRPM4 inhibitors. In addition, we found that compound **5** possessed a dual function as a TRPM4 inhibitor and also as a chemical chaperon rescuing the membrane expression of a loss-of-expression TRPM4 variant.

Compound 5 as a potential inhibitor of TRPM4

Recently, virtual screening methods have emerged as an efficient approach for identifying potent and specific inhibitors for different ion channels (Langer and Krovat, 2003; Fernández-Ballester et al., 2011 Simonin et al., 2015). In this study we carried out an initial virtual screening using an in-house developed pharmacophore similarity search algorithm: xLOS, which compared the spatial overlap between a catalog of commercially available drug-like small molecules to the three reference TRPM4 inhibitors, 9-phenanthrol, glibenclamide and FFA. The purchased compounds selected from the top scoring list were further validated using a new fluorescence based Na^+ sensitive screening assay, which measured the activity of TRPM4 in a stably expressing cell line. This screening identified two aryloxyacyl-anthranilic acid compounds **4** and **5** as the most potent compounds with IC_{50} in ~1 µM

range, which is several fold lower compared to all the reference inhibitors (Abriel et al., 2012). It is noteworthy that compound **5** inhibited TRPM4 current in both overexpressed cell line and endogenously expressed in prostate cancer cell line with similar potency and presented selectivity over other TRP family members including TRPM5, TRPM7, TRPM8, TRPV1, TRPV3, TRPV6 . Analysis of our *in silico* and cell based results highlighted compound **5** as having a good balance of potency and selectivity which encouraged us for further optimization of this compound through chemical modifications. Although, altering substituents on aromatic rings and within the acetyl linker often abolished the inhibition activity, we did identified compound **6** with increased potency of < 1 µM IC_{50} inhibition (***Table 1, and Supporting information Table S1-S3***). However, due to off target effect of compound **6** on GLPR1 receptor as predicted by polypharmacology browser, we did not perform any further experiments with this compound. Future optimization studies on compound **6** could provide a promising tool compound for TRPM4 pharmacology.

Success in finding these inhibitors demonstrates the capability of combining *in silico* and Na^+ sensitive screening assay to explore focused chemical landscapes to identify potent and specific inhibitors of TRPM4. The chemical diversity surveyed here in the virtual screening and subsequent SAR study is summarized in ***Figure 8*** with a color-coded map of the chemical space covered by the compounds tested, plotted with our recently reported web-based tool WebMolCS (Awale et al., 2017) using the principle of similarity mapping (Awale and Reymond, 2015). This 3D-map positions molecules as individual spheres in a space where distances represent the relative similarities of molecules to one another, as measured by the Tanimoto coefficient of a 1024-bit binary Daylight type substructure fingerprint, which perceives detailed features of the molecules (Hagadone, 1992). Each sphere is color-coded according to the observed TRPM4 activities (inactive = blue, most active = red). This representation illustrates that the anthranilic acid TRPM4 inhibitors occupy a chemical space significantly shifted from the reference inhibitors 9-phenanthrol, FFA and glibenclamide used for LBVS. Furthermore, the map shows that only very few analogs of 9-phenanthrol were actually tested due to limited commercial availability.

Compound 5 as a potential chemical chaperone for TRPM4 loss-of-expression variant

A number of mutations in the human *TRPM4* gene linked with various cardiac pathologies have led to reduced membrane expression and function either due to misfolding or improper assembly of the channel protein (Stallmeyer et al., 2012; Syam et al., 2016). In past decade, several studies used *in silico* and *in vitro* screening to identify small molecules that can partially rescue the trafficking defect of many proteins (Naik et al., 2012) including ion channels such as CFTR (Van Goor et al., 2006; Rowe and Verkman, 2013). Most of these chemical chaperones had shown certain selectivity toward the target either by direct interactions or via other accessory proteins. We reasoned that, since compound **5** outlays better potency, selectivity and lower cytotoxicity, it could be a potential candidate to be used as chemical chaperone for A432T-TRPM4 mutant channel. Indeed compound **5** rescued the total and surface expression of both the core and fully glycosylated forms of the A432T variant channel. This chemical chaperoning effect may be related to a compound-dependent increase in protein stability. Moreover, the observed increase in A432T-TRPM4-mediated current upon compound **5** pre-incubation, followed by a washout protocol, is consistent with an increased number of channels at the cell surface. The partial functional rescuing may be explained by either mutation-dependent altered gating or only partial washout of the compound **5.** However, it is notable that this rescuing effect was specific to the structure of compound **5**, since an inactive congener of **5** with no inhibitory activity, i.e., **51**, did not show any rescuing effect. It was also channel specific since **5** did not rescue a loss-of-expression hERG channel variant. These results suggest that this positive effect could be from a direct and selective interaction of compound **5** with the TRPM4 protein and hence reducing its degradation by the endoplasmic reticulum-associated degradation process. Note that at this stage, there is no evidence that the protein binding of **5** leading to TRPM4 inhibition is identical to the one resulting in its rescuing. Nevertheless, to the best of our knowledge, this is the first report of a small molecule compound functionally rescuing the membrane expression of a TRP channel loss-of-expression variant.

In conclusion, this study demonstrates that using the newly developed xLOS method linked to a Na^+-sensitive screening assay, a series of halogenated anthranilic amide compounds with potent and selective TRPM4 inhibition properties was discovered. The highly potent compounds **4**, **5** and **6** that

we identified in this study will open new ways in TRPM4 pharmacology. In the context of recent structural data of TRPM4 (Guo et al., 2017; Winkler et al., 2017; Autzen et al., 2018), future structure-function relationship studies coupled with our selective and potent inhibitor compound **5** will benefit for better understanding of channel function. Moreover, compound **5** demonstrated not only selective inhibition but also chemical chaperone property, which provide a good starting point for developing clinical drug candidates for rescuing loss-of-expression variants.

MATERIALS AND METHODS

Ligand-based virtual screening

First round of virtual screening (VS) was performed in the Princeton database, which contains 900,000 purchasable compounds, using three different reference compounds, namely 9-phenanthrol, glibenclamide and flufenamic acid. The VS was carried out with an in-house developed extended Ligand Overlap Score (xLOS) method, which computes the 3D-shape and –pharmacophore similarity between any two compounds (typically reference and database compounds)(Simonin et al., 2015). The single lowest energy 3D-models of reference and database molecules were generated using CORINA program available from Molecular Networks Pvt. Ltd. XLOS used these 3D-models to calculate a 3D-similarity score between the reference compound and the database molecules. Afterward, for each of the three reference molecules, 235 molecules were visually selected from the top 1000 xLOS scoring compounds, 214 of those were purchased from Princeton Biomolecular Research. These compounds were dissolved in DMSO solution and tested on TRPM4 activity. Next, three hits from this first round of VS were used for a second round of VS in the Princeton database using xLOS. From this second round, 247 compounds were selected and purchased for biological testing.

Visualization of screening library in 3D

The visualization of screening library was facilitated by an in-house developed webMolCS web server (www.gdb.unibe.ch). WebMolCS takes a user-defined list of molecules (in SMILES format) as input and produces interactive color-coded 3D-maps using either principal component analysis or similarity mapping of any of the six different molecular fingerprints used for molecular representation. In the present study, similarity mapping (Sim map) and substructures fingerprint (sFP) were used to generate the 3D-maps. The colors of the 3D-maps shown in ***Figure 1*** represent the similarity (calculated using sFP fingerprint) of the screened compounds to the best compound **6** from synthetic optimization; from low to high similarity: blue-cyan-green-yellow (Awale and Reymond, 2017).

Chemical synthesis of compounds

The synthesis and characterization of all compounds are described in the Supplementary methods.

Cell culture

HEK293 and tetracycline-inducible HEK293 Flag-TRPM4-expressing cells were used. The HEK293 cells were a gift from Dr. R.S. Kass, Columbia University, New York, USA. These cells were given to the group of Dr. R.S. Kass by Dr. B. Stillman, Cold Spring Harbor Laboratories, Cold Spring, USA. Tetracycline-inducible HEK293 Flag-TRPM4 cells were a gift from Dr. P. Bouvagnet (University of Lyon, France). These cells were cultured at 37 °C in DMEM supplemented with 10% fetal bovine serum (FBS, Invitrogen, CA, USA), 4 mM glutamine (Sigma), 5 µg/mL S-blasticidin (Invitrogen) and 0.4 mg/mL Zeocin (Invitrogen). TRPM4 expression was induced by adding 1 µg/mL of tetracycline to induction medium (DMEM without phenol red (Gibco 31053, Paisley, UK) supplemented with 10% FBS (Invitrogen) and 2% L-Glutamin (Sigma)) 15-20 hours before the experiment. For TRPM4 variant studies, HEK293 cells cultured at 37 °C in DMEM supplemented with 10% FBS and 4 mM glutamine were transiently transfected with 250 ng of HA-tagged TRPM4 WT or HA-tagged TRPM4 p.A432T in a 100 mm dish, mixed with 4 µL of JetPEI (Polyplus transfection, Illkirch, France) and 46 µL of 150 mM NaCl. The cells were incubated for 24 h at 37 °C

with 5% CO_2. All transfections included 100 ng of eGFP as a reporter gene. Cells were used 24 hours after transfection. Lymph node carcinoma of the prostate (LNCaP) cells was purchased from the American Type Cell Culture Collection (ATCC, Rockville, MD, USA) and cultured in RPMI Medium 1640 (Gibco) supplemented with 10% FCS and 1% penicillin/streptomycin (Invitrogen).

TRPM4 KD cell line has been provided by Transposagen Biopharmaceuticals (Lexington, KY, USA) and generated using CRISPR/Cas9 technique. The cells had been transfected with both the Cas9 vector and the corresponding U6 expressed sgRNA vector in a 1:1 molar ratio. Transfection was done with Lipofectamine 2000 (ThermoFischer Scientific, MA, USA) following the manufacturer's protocols. Loss of TRPM4 gene function and protein was then checked in single clone`s amplified using qPCR and western blot. The selected clone were cultured and expanded in condition similar for HEK293 as mentioned above.

sgRNA targets:

TRPM4 TS1	GCCACCTCGCCGCTCTCGC
TRPM4 TS2	GCTCCAGGGGGCCTGCCCG

Compound cytotoxicity assay

Cytotoxicity of compounds **4**, **5** and **6** were studied in RAW 264.7 and HeLa cells for anti-proliferative effects. The cells were seeded at 2'000 cells per well in 100 µL culture media in a 96-well plate. Following overnight incubation different concentrations of the compounds were added and incubated together with the solvent control for 72 hour at 37 °C. After that, the cells were incubated with MTT (3-(4,5-dimethylthiazol-2-yl)-2,5-diphenyltetrazolium bromide, final concentration 0.5 mg/mL) for 4 hour at 37 °C and solubilized with DMSO. The plates were measured at 550 nm (absorbance) and the IC50 value related to cell survival/proliferation was calculated and plotted. Paclitaxel was used as positive control. Experiments were performed in at least three independent experiments, each in triplicate.

Western blot

To detect TRPM4 protein expression, whole-cell lysates were prepared by lysing cells in lysis buffer (50 mM HEPES pH 7.4; 150 mM NaCl; 1.5 mM $MgCl_2$: 1 mM EGTA pH 8.0; 10 % glycerol; 1% Triton X-100; 1X Complete protease inhibitor cocktail (Roche, Mannheim, Germany)) for 1 hour at 4 °C. Cell lysates were centrifuged for 15 minutes at 16,000 g at 4 °C and protein concentration was evaluated using Bradford assay. 60 µg of each protein sample was run on 9 % polyacrylamide gels, later transferred with the TurboBlot dry blot system (Biorad, Hercules, CA, USA). After transfer membrane were blocked with 0.1% BSA in PBS and incubated with Primary antibodies anti-TRPM4 (generated by Pineda, Berlin, Germany) and anti-α-actin A2066 (Sigma-Aldrich, St. Louis, Missouri, USA) using SNAP i.d. system (Millipore, Billerica, MA, USA), followed by an incubation with secondary antibody, IRDye 800CW, (LI-COR Biosciences, Lincoln, NE, USA). Membrane were scanned using LiCor Odyssey Infrared imaging system (LiCor Biosciences, Lincoln, NE, USA) and protein band intensity was quantified using Image Studio Lite software from LiCor Biosciences.

For detecting TRPM4 WT and A432T variant whole-cell (total) and surface expression after incubation with compound **5,** the cells were washed twice with cold 1X PBS and treated with EZlinkTM Sulfo-NHS-SS-Biotin (Thermo Scientific, Waltham, MA, USA) 0.5 mg/mL in cold 1X PBS for 15 minutes at 4°C. Subsequently, the cells were washed twice with 200 mM Glycine in cold 1X PBS and twice with cold 1X PBS to inactivate and to remove the excess biotin, respectively. The cells were then lysed with 1X lysis buffer for 1 hour at 4°C. Cell lysates were centrifuged at 16,000 g at 4°C for 15 minutes. Two milligrams of the supernatant were incubated with 50 µL Streptavidin Sepharose High Performance beads (GE Healthcare, Uppsala, Sweden) for 2 hours at 4°C, and the remaining supernatant was kept as the input. The beads were subsequently washed five times with 1X lysis buffer before elution with 50 µL of 2X NuPAGE sample buffer (Invitrogen, Carlsbad, CA, USA) plus 100 mM DTT at 37°C for 30 minutes. These biotinylated fractions were analyzed as TRPM4 expressed at the cell surface. The input fractions, analyzed as total expression of TRPM4, were resuspended with 4X NuPAGE Sample Buffer plus 100 mM DTT to give a concentration of 1 mg/mL and incubated at 37 °C for 30 minutes.

Na^+-influx screening assay

TRPM4-expressing cells were plated in 96-well black-walled clear bottomed poly-D-lysine coated plates (Corning, NY, USA) at a density of 30,000 cells / well in 100 µL of induction medium (described above). After plating, cells were incubated for 48 hours at 37 °C in a 5% CO_2 incubator. On the day of assay, the induction medium was replaced with 100 µL/well of the assay buffer (in mM: 140 NMDG-Cl, 10 KCl, 1 $CaCl_2$, 1 $MgCl_2$, 10 HEPES (pH 7.2) with NMDG-OH and 290 to 300 mOsM) and incubated for 45 minutes at room temperature (RT). Later, the assay buffer was replaced with 95 µL/well of dye loading solution prepared in assay buffer supplemented with 0.1% pluronic acid F-127 (Teflabs, TX, USA) and 5 µM of Na^+ sensitive dye, Asante Natrium Green – II (ANGII) (Teflabs). The cells were incubated in the dark at RT for 45 minutes. After incubation, the dye loading solution was completely drained and replaced with 72 µL assay buffer and incubated in the dark for 20 minutes, followed by fluorescence readout on FLIPR $^{TETRA®}$ (Molecular devices, CA, USA).

For evaluation of the effects of TRPM4 inhibitors using the Na^+ influx assay, a 10X compound plate were prepared in assay buffer in 96-well polystyrene plates (Corning, NY, USA). All stocks were dissolved in DMSO. To initiate Na^+ influx through activation of TRPM4, a 5X stimulus buffer plate containing (in mM) 700 NaCl, 4 $CaCl_2$, 4 $MgCl_2$, 40 HEPES, (pH 7.2 with NaOH) along with 50 µM of ionomycin prepared in a 96-well polystyrene plate (Corning, NY, USA). The background control wells contained stimulus buffer without ionomycin (W/O).

Fluorophores were excited by the 488 nm line of an argon laser. Emission was filtered with a 540 ± 30 nm bandpass filter. Initial baseline fluorescence was measured at 1 Hz from the plate loaded with ANGII dye for 1 minute. Followed by addition of 8 µL solution from 10X compound plate, fluorescence was monitored at an interval of 1 Hz for 5 minutes. Finally, to activate TRPM4, 20 µL of solution from the stimulus buffer plate was added, and fluorescence was acquired at 0.5 Hz intervals during and after addition for 5 minutes. Data from individual assay wells were normalized to initial baseline fluorescence. The initial rise in fluorescence was measured as area under the curve, and the counts were normalized using the formula {[(Ionomycin - Compound)/ (Ionomycin – W/O

Ionomycin)] * 100} to plot concentration-response curves for inhibitor hits. The experimenter for the screening experiments (L.C.O) was blinded and was not aware of any chemical properties of the compounds until the best hits were validated. The steps are summarized as workflow mentioned in ***table 2***.

Electrophysiology

Cells were plated in 35 mm poly-D-lysine coated dishes (Corning, NY, USA) in induction medium (phenol red free DMEM medium (GIBCO-31053)) supplemented with 10 % FBS and 1 µg/mL tetracycline (Invitrogen, USA). After plating, cells were incubated for 48 hours at 37 °C in a 5% CO_2 incubator. Electrophysiological recordings were performed in the inside-out patch clamp configuration with patch pipettes (1-2 µm tip opening) pulled from 1.5 mm borosilicate glass capillaries (World Precision Instruments, Inc. Fl, USA) using DMZ Universal puller (Zeitz-Instruments, GmbH, München, Germany). Pipette tips were polished to have a pipette resistance of 2–4 M Ω in the bath solution. The pipette solution contained (in mM) 150 NaCl, 10 HEPES, 2 $CaCl_2$ (pH 7.4 with NaOH). The bath solution contained (in mM) 150 NaCl 10 HEPES, 2 HEDTA (pH 7.4 with NaOH) as Ca^{2+}-free solutions. Solutions containing 0.1 to 2 mM Ca^{2+} were prepared by adding the appropriate concentration of $CaCl_2$ without a Ca^{2+} chelator to a solution containing (in mM) 150 NaCl, 10 HEPES (pH 7.4 with NaOH) as reported previously (Zhang et al., 2005). Bath solutions with different Ca^{2+} concentrations were applied to cells by a modified rapid solution exchanger (Perfusion Fast-Step SF-77B; Warner Instruments Corp. CT, USA). Inhibitors in DMSO stock were diluted to appropriate concentrations in the pipette solution and applied on extracellular side of the cells. Membrane currents were recorded with a Multiclamp 700B amplifier (Molecular devices, CA, USA) controlled by Clampex 10 via a Digidata 1332A (Molecular devices, CA, USA). Data were low-pass filtered at 5 kHz and sampled at 10 kHz. Experiments were performed at RT (20–25 °C). For I-V relations, currents were recorded using a stimulation protocol consisting of voltage steps of 200 ms from a holding potential of 0 mV ranging from -80 mV to +100 mV, followed by a tail voltage at -100 mV. For constructing concentration-response curves, steady-state current at +100 mV recorded in 300 µM Ca^{2+} were normalized to current in absence of any inhibitor. For rescue experiments with

compound **5**, before performing patch clamp recordings the culture medium was replaced with bath solution without any added inhibitor.

For whole-cell patch clamp on LNCaP cells, 50 ms voltage ramps spanning -100 to +100 mV were delivered every 2 s from a holding potential of 0 mV. Whole-cell currents were recorded with a HEKA patch clamp system (EPC-10, HEKA Elektronik Dr. Schutze GmbH, Rhein, Germany). Series resistance (Rs) was monitored in response to a 5 mV voltage step and compensated online up to 80% if needed. Bath solution contained (in mM): 140 NaCl, 0.5 $CaCl_2$, 3 $MgCl_2$, 10 HEPES. Glucose was added to adjust osmolarity to 330 mOsmol/L and pH was adjusted to 7.2 with NaOH. Pipette solution contained (in mM): 140 Cs-glutamate, 10 HEDTA, 10 HEPES, 8 NaCl, 12.24 $MgCl_2$, and 0.00049 $CaCl_2$. Free Mg^{2+} of 3 mM and 10 µM Ca^{2+} was calculated according to http://web.stanford.edu/~cpatton/webmaxcS.htm. Whole-cell currents at -80 and +80 mV were extracted, normalized to the cell capacity, and plotted versus time.

Data analysis

To quantify the Na^+ influx after addition of stimulus buffer, the area under the curve (AUC) was calculated using the ScreenWorks™ software (Molecular devices, CA, USA). Data points acquired from the Na^+ influx assay from FLIPR or electrophysiology data were exported and analyzed using IGOR PRO 6 (Wavematrix, OR, USA). Z` factor was calculated as described earlier (Zhang et al., 1999), using the following equation: $Z` = 1 - [(3SD_p + 3SD_n) / (3Mean_p - 3Mean_n)]$ where SD is standard deviation, and p and n are positive and negative control, respectively. Michaelis-Menten constant for Na^+ dependence of the signal was deduced using the following equation: $V = [Vmax [S] / (K_m + [S])]$, where V_{max} is maximal fluorescence signal, S is Na^+ concentration and K_m is Michaelis-Menten constant. Concentration-response curves were fitted using the Hill equation fit parameter of IGOR ($NC = NCmax [Cmpd]^{nH} / \{[Cmpd]^{nH} + EC_{50}{}^{nH}\}$), where NC is normalized current or counts, [Cmpd] is compound concentration and nH is the Hill coefficient. Data are presented as mean ± SEM except for ***Figure 2Ai and Aii***, where each data point n = 2 and data are presented as mean ± SD. Statistically significant difference between means were determined using students`s *t* test for

comparison between two means with $n \geq 5$. $P \leq 0.05$ were accepted as significant and represented as * in respective figure panels. The data and statistical analyses comply with the recommendations on experimental design and analysis in pharmacology (Curtis et al., 2015).

Nomenclature of Targets and Ligands

Key protein targets and ligands in this article are hyperlinked to corresponding entries in http://www.guidetopharmacology.org, the common portal for data from the IUPHAR/BPS Guide to PHARMACOLOGY(Harding et al., 2018), and are permanently archived in the Concise Guide to PHARMACOLOGY 2017/18 (Alexander Stephen PH et al., 2017).

Author Contributions: L.C.O, C.D, B.B, G.N, S.K, M.R, J.G, M.L, C.P, J.L.R, H.A designed the experiments. L.C.O developed and validated screening assay. L.C.O and M.R performed compound screening. L.C.O and S.K performed and analyzed patch clamp experiments. B.B performed western blots for chemical chaperone experiments. U.T performed additional compound selectivity profiling and D.R-K performed biotinylation experiments. C.D, G.N, C.S performed virtual screening, purchased compounds. C.D, G.N performed chemical synthesis for SAR studies. L.C.O, J.L.R, H.A wrote the manuscript with extensive comments from C.D, B.B, G.N, M.R, J.G, S.K, M.L, C.P, J.L.R, H.A.

Conflict of interest: The authors declare no conflicts of interest.

REFERENCES

Abriel, H., Syam, N., Sottas, V., Amarouch, M.Y., and Rougier, J.-S. (2012). TRPM4 channels in the cardiovascular system: physiology, pathophysiology, and pharmacology. Biochem. Pharmacol. *84*: 873–881.

Alexander, S.P.H., Benson, H.E., Faccenda, E., Pawson, A.J., Sharman, J.L., Catterall, W.A., et al. (2013). The Concise Guide to PHARMACOLOGY 2013/14: ion channels. Br. J. Pharmacol. *170*: 1607–1651.

Alexander Stephen PH, Striessnig Jörg, Kelly Eamonn, Marrion Neil V, Peters John A, Faccenda Elena, et al. (2017). THE CONCISE GUIDE TO PHARMACOLOGY 2017/18: Voltage-gated ion channels. Br. J. Pharmacol. *174*: S160–S194.

Amarouch, M.-Y., Syam, N., and Abriel, H. (2013). Biochemical, single-channel, whole-cell patch clamp, and pharmacological analyses of endogenous TRPM4 channels in HEK293 cells. Neurosci. Lett. *541*: 105–110.

Ashida, S., Nakagawa, H., Katagiri, T., Furihata, M., Iiizumi, M., Anazawa, Y., et al. (2004). Molecular features of the transition from prostatic intraepithelial neoplasia (PIN) to prostate cancer: genome-wide gene-expression profiles of prostate cancers and PINs. Cancer Res. *64*: 5963–5972.

Autzen, H.E., Myasnikov, A.G., Campbell, M.G., Asarnow, D., Julius, D., and Cheng, Y. (2018). Structure of the human TRPM4 ion channel in a lipid nanodisc. Science *359*: 228–232.

Awale, M., Probst, D., and Reymond, J.-L. (2017). WebMolCS: A Web-Based Interface for Visualizing Molecules in Three-Dimensional Chemical Spaces. J. Chem. Inf. Model. *57*: 643–649.

Awale, M., and Reymond, J.-L. (2014). A multi-fingerprint browser for the ZINC database. Nucleic Acids Res. *42*: W234-239.

Awale, M., and Reymond, J.-L. (2015). Similarity Mapplet: Interactive Visualization of the Directory of Useful Decoys and ChEMBL in High Dimensional Chemical Spaces. J. Chem. Inf. Model. *55*: 1509–1516.

Awale, M., and Reymond, J.-L. (2017). The polypharmacology browser: a web-based multi-fingerprint target prediction tool using ChEMBL bioactivity data. J. Cheminformatics *9*:.

Berg, K.D., Soldini, D., Jung, M., Dietrich, D., Stephan, C., Jung, K., et al. (2016). TRPM4 protein expression in prostate cancer: a novel tissue biomarker associated with risk of biochemical recurrence following radical prostatectomy. Virchows Arch. Int. J. Pathol. *468*: 345–355.

Burris, S.K., Wang, Q., Bulley, S., Neeb, Z.P., and Jaggar, J.H. (2015). 9-Phenanthrol inhibits recombinant and arterial myocyte TMEM16A channels. Br. J. Pharmacol. *172*: 2459–2468.

Curtis, M.J., Bond, R.A., Spina, D., Ahluwalia, A., Alexander, S.P.A., Giembycz, M.A., et al. (2015). Experimental design and analysis and their reporting: new guidance for publication in BJP. Br. J. Pharmacol. *172*: 3461–3471.

Demion, M., Bois, P., Launay, P., and Guinamard, R. (2007). TRPM4, a Ca2+-activated nonselective cation channel in mouse sino-atrial node cells. Cardiovasc. Res. *73*: 531–538.

Denning, G.M., Anderson, M.P., Amara, J.F., Marshall, J., Smith, A.E., and Welsh, M.J. (1992). Processing of mutant cystic fibrosis transmembrane conductance regulator is temperature-sensitive. Nature *358*: 761–764.

Feng, T.-C., Cui, C.-Z., Dong, F., Feng, Y.-Y., Liu, Y.-D., and Yang, X.-M. (2012). Phenanthrene biodegradation by halophilic Martelella sp. AD-3. J. Appl. Microbiol. *113*: 779–789.

Fernández-Ballester, G., Fernández-Carvajal, A., González-Ros, J.M., and Ferrer-Montiel, A. (2011). Ionic Channels as Targets for Drug Design: A Review on Computational Methods. Pharmaceutics *3*: 932–953.

Fonfria, E., Murdock, P.R., Cusdin, F.S., Benham, C.D., Kelsell, R.E., and McNulty, S. (2006). Tissue distribution profiles of the human TRPM cation channel family. J. Recept. Signal Transduct. Res. *26*: 159–178.

Gardam, K.E., Geiger, J.E., Hickey, C.M., Hung, A.Y., and Magoski, N.S. (2008). Flufenamic acid affects multiple currents and causes intracellular Ca2+ release in Aplysia bag cell neurons. J. Neurophysiol. *100*: 38–49.

Garland, C.J., Smirnov, S.V., Bagher, P., Lim, C.S., Huang, C.Y., Mitchell, R., et al. (2015). TRPM4 inhibitor 9-phenanthrol activates endothelial cell intermediate conductance calcium-activated potassium channels in rat isolated mesenteric artery. Br. J. Pharmacol. *172*: 1114–1123.

Gaulton, A., Bellis, L.J., Bento, A.P., Chambers, J., Davies, M., Hersey, A., et al. (2012). ChEMBL: a large-scale bioactivity database for drug discovery. Nucleic Acids Res. *40*: D1100-1107.

Grand, T., Demion, M., Norez, C., Mettey, Y., Launay, P., Becq, F., et al. (2008). 9-phenanthrol inhibits human TRPM4 but not TRPM5 cationic channels. Br. J. Pharmacol. *153*: 1697–1705.

Grilo, L.S., Pruvot, E., Grobéty, M., Castella, V., Fellmann, F., and Abriel, H. (2010). Takotsubo cardiomyopathy and congenital long QT syndrome in a patient with a novel duplication in the Per-Arnt-Sim (PAS) domain of hERG1. Heart Rhythm *7*: 260–265.

Guinamard, R., Hof, T., and Del Negro, C.A. (2014). The TRPM4 channel inhibitor 9-phenanthrol. Br. J. Pharmacol. *171*: 1600–1613.

Guo, J., She, J., Zeng, W., Chen, Q., Bai, X.-C., and Jiang, Y. (2017). Structures of the calcium-activated, non-selective cation channel TRPM4. Nature *552*: 205–209.

Hagadone, T.R. (1992). Molecular substructure similarity searching: efficient retrieval in two-dimensional structure databases. J. Chem. Inf. Comput. Sci. *32*: 515–521.

Harding, S.D., Sharman, J.L., Faccenda, E., Southan, C., Pawson, A.J., Ireland, S., et al. (2018). The IUPHAR/BPS Guide to PHARMACOLOGY in 2018: updates and expansion to encompass the new guide to IMMUNOPHARMACOLOGY. Nucleic Acids Res. *46*: D1091–D1106.

Holzmann, C., Kappel, S., Kilch, T., Jochum, M.M., Urban, S.K., Jung, V., et al. (2015). Transient receptor potential melastatin 4 channel contributes to migration of androgen-insensitive prostate cancer cells. Oncotarget *6*: 41783–41793.

Hopkins, A.L., Keserü, G.M., Leeson, P.D., Rees, D.C., and Reynolds, C.H. (2014). The role of ligand efficiency metrics in drug discovery. Nat. Rev. Drug Discov. *13*: 105–121.

Kilch, T., Kappel, S., and Peinelt, C. (2016). Regulation of Ca(2+) signaling in prostate cancer cells. Channels Austin Tex *10*: 170–171.

Kilchmann, F., Marcaida, M.J., Kotak, S., Schick, T., Boss, S.D., Awale, M., et al. (2016). Discovery of a Selective Aurora A Kinase Inhibitor by Virtual Screening. J. Med. Chem. *59*: 7188–7211.

Kruse, M., and Pongs, O. (2014). TRPM4 channels in the cardiovascular system. Curr. Opin. Pharmacol. *15*: 68–73.

Kruse, M., Schulze-Bahr, E., Corfield, V., Beckmann, A., Stallmeyer, B., Kurtbay, G., et al. (2009). Impaired endocytosis of the ion channel TRPM4 is associated with human progressive familial heart block type I. J. Clin. Invest. *119*: 2737–2744.

Langer, T., and Krovat, E.M. (2003). Chemical feature-based pharmacophores and virtual library screening for discovery of new leads. Curr. Opin. Drug Discov. Devel. *6*: 370–376.

Launay, P., Fleig, A., Perraud, A.-L., Scharenberg, A.M., Penner, R., and Kinet, J.-P. (2002). TRPM4 Is a Ca2+-Activated Nonselective Cation Channel Mediating Cell Membrane Depolarization. Cell *109*: 397–407.

Liu, H., Chatel, S., Simard, C., Syam, N., Salle, L., Probst, V., et al. (2013). Molecular genetics and functional anomalies in a series of 248 Brugada cases with 11 mutations in the TRPM4 channel. PloS One *8*: e54131.

Liu, H., El Zein, L., Kruse, M., Guinamard, R., Beckmann, A., Bozio, A., et al. (2010). Gain-of-function mutations in TRPM4 cause autosomal dominant isolated cardiac conduction disease. Circ. Cardiovasc. Genet. *3*: 374–385.

Makar, T.K., Gerzanich, V., Nimmagadda, V.K.C., Jain, R., Lam, K., Mubariz, F., et al. (2015). Silencing of Abcc8 or inhibition of newly upregulated Sur1-Trpm4 reduce inflammation and disease progression in experimental autoimmune encephalomyelitis. J. Neuroinflammation *12*: 210.

Malhotra, S., Castilló, J., Negrotto, L., Merino-Zamorano, C., Montaner, J., Vidal-Jordana, A., et al. (2013). TRPM4 mRNA expression levels in peripheral blood mononuclear cells from multiple sclerosis patients. J. Neuroimmunol. *261*: 146–148.

Naik, S., Zhang, N., Gao, P., and Fisher, M.T. (2012). On the Design of Broad Based Screening Assays to Identify Potential Pharmacological Chaperones of Protein Misfolding Diseases. Curr. Top. Med. Chem. *12*: 2504–2522.

Nilius, B., Prenen, J., Droogmans, G., Voets, T., Vennekens, R., Freichel, M., et al. (2003). Voltage Dependence of the Ca2+-activated Cation Channel TRPM4. J. Biol. Chem. *278*: 30813–30820.

Palmer, R.K., Atwal, K., Bakaj, I., Carlucci-Derbyshire, S., Buber, M.T., Cerne, R., et al. (2010). Triphenylphosphine oxide is a potent and selective inhibitor of the transient receptor potential melastatin-5 ion channel. Assay Drug Dev. Technol. *8*: 703–713.

Prevarskaya, N., Zhang, L., and Barritt, G. (2007). TRP channels in cancer. Biochim. Biophys. Acta *1772*: 937–946.

Rowe, S.M., and Verkman, A.S. (2013). Cystic Fibrosis Transmembrane Regulator Correctors and Potentiators. Cold Spring Harb. Perspect. Med. *3*:.

Sagredo, A.I., Sagredo, E.A., Cappelli, C., Báez, P., Rodrigo, A.M., Blanco, C., et al. (2017). TRPM4 regulates Akt/GSK3-β activity and enhances β-catenin signaling and cell proliferation in prostate cancer cells. Mol. Oncol.

Schattling, B., Steinbach, K., Thies, E., Kruse, M., Menigoz, A., Ufer, F., et al. (2012). TRPM4 cation channel mediates axonal and neuronal degeneration in experimental autoimmune encephalomyelitis and multiple sclerosis. Nat. Med. *18*: 1805–1811.

Schinke, E.N., Bii, V., Nalla, A., Rae, D.T., Tedrick, L., Meadows, G.G., et al. (2014). A novel approach to identify driver genes involved in androgen-independent prostate cancer. Mol. Cancer *13*: 120.

Schneider, G., Neidhart, W., Giller, T., and Schmid, G. (1999). "Scaffold-Hopping" by Topological Pharmacophore Search: A Contribution to Virtual Screening. Angew. Chem. Int. Ed. *38*: 2894–2896.

Scior, T., Bender, A., Tresadern, G., Medina-Franco, J.L., Martínez-Mayorga, K., Langer, T., et al. (2012). Recognizing pitfalls in virtual screening: a critical review. J. Chem. Inf. Model. *52*: 867–881.

Simard, C., Sallé, L., Rouet, R., and Guinamard, R. (2012). Transient receptor potential melastatin 4 inhibitor 9-phenanthrol abolishes arrhythmias induced by hypoxia and re-oxygenation in mouse ventricle. Br. J. Pharmacol. *165*: 2354–2364.

Simonin, C., Awale, M., Brand, M., Deursen, R. van, Schwartz, J., Fine, M., et al. (2015). Optimization of TRPV6 Calcium Channel Inhibitors Using a 3D Ligand-Based Virtual Screening Method. Angew. Chem. Int. Ed Engl. *54*: 14748–14752.

Singh, J., Manickam, P., Shmoish, M., Natik, S., Denyer, G., Handelsman, D., et al. (2006). Annotation of androgen dependence to human prostate cancer-associated genes by microarray analysis of mouse prostate. Cancer Lett. *237*: 298–304.

Stallmeyer, B., Zumhagen, S., Denjoy, I., Duthoit, G., Hébert, J.-L., Ferrer, X., et al. (2012). Mutational spectrum in the Ca(2+)--activated cation channel gene TRPM4 in patients with cardiac conductance disturbances. Hum. Mutat. *33*: 109–117.

Sterling, T., and Irwin, J.J. (2015). ZINC 15 – Ligand Discovery for Everyone. J. Chem. Inf. Model. *55*: 2324–2337.

Suguro, M., Tagawa, H., Kagami, Y., Okamoto, M., Ohshima, K., Shiku, H., et al. (2006). Expression profiling analysis of the CD5+ diffuse large B-cell lymphoma subgroup: Development of a CD5 signature. Cancer Sci. *97*: 868–874.

Syam, N., Chatel, S., Ozhathil, L.C., Sottas, V., Rougier, J.-S., Baruteau, A., et al. (2016). Variants of Transient Receptor Potential Melastatin Member 4 in Childhood Atrioventricular Block. J. Am. Heart Assoc. *5*:.

Ullrich, N.D., Voets, T., Prenen, J., Vennekens, R., Talavera, K., Droogmans, G., et al. (2005). Comparison of functional properties of the Ca2+-activated cation channels TRPM4 and TRPM5 from mice. Cell Calcium *37*: 267–278.

Van Goor, F., Straley, K.S., Cao, D., González, J., Hadida, S., Hazlewood, A., et al. (2006). Rescue of DeltaF508-CFTR trafficking and gating in human cystic fibrosis airway primary cultures by small molecules. Am. J. Physiol. Lung Cell. Mol. Physiol. *290*: L1117-1130.

Winkler, P.A., Huang, Y., Sun, W., Du, J., and Lü, W. (2017). Electron cryo-microscopy structure of a human TRPM4 channel. Nature *552*: 200–204.

Zhang, J.-H., Chung, T.D.Y., and Oldenburg, K.R. (1999). A Simple Statistical Parameter for Use in Evaluation and Validation of High Throughput Screening Assays. J. Biomol. Screen. *4*: 67–73.

Zhang, Z., Okawa, H., Wang, Y., and Liman, E.R. (2005). Phosphatidylinositol 4,5-Bisphosphate Rescues TRPM4 Channels from Desensitization. J. Biol. Chem. *280*: 39185–39192.

Zhou, Z., Gong, Q., and January, C.T. (1999). Correction of defective protein trafficking of a mutant HERG potassium channel in human long QT syndrome. Pharmacological and temperature effects. J. Biol. Chem. *274*: 31123–31126.

TABLE:

TRPM4 inhibitors

ID	Na^+ influx IC_{50} (µM)	Electrophysiology IC_{50} (µM)	R_1	R_2	R_3
4	1.6 ± 0.3	1.0 ± 0.2	Cl	CH_3	2-CH_3-4-Cl
5	1.5 ± 0.1	1.8 ± 0.1	Cl	H	2-Cl
11	1.0 ± 0.2	1.6 ± 0.5	Br	H	2-Cl
12	1.8 ± 0.2		Cl	CH_3	2,4-diCl
13	1.8 ± 0.1		Cl	H	2,4-diBr
14	3.4 ± 1.1		Cl	H	2,4-diF
15	2.6 ± 0.3		Cl	H	2-Cl-5-nitro
16	2.6 ± 0.4		Cl	H	3-phenyl
6	0.4 ± 0.3	0.2 ± 0.07			
7	2.2 ± 0.4				
8	8.3 ± 0.7				
9	5.9 ± 0.5				
10	1.2 ± 0.5				
9P	29.1 ± 5.8	17.0 ± 2.8			

Table 1. IC_{50} values of TRPM4 inhibitors tested using the Na^+ influx screening assay and electrophysiology recordings.(9P- 9 Phenanthrol)

ASSAY WORKFLOW

No.	Step	Value	Detail
1	Cell plating and induction	100 µL	30,000 cells/well Incubation for 48 hours
		Drain the content	

2	Na^+ depletion	100 µL	Assay buffer Incubation for 45 mins
		Drain the content	
3	Dye loading	95 µL	ANGII dye prepared in assay buffer Incubation in dark for 45 mins at RT
		Drain the content	
4	Assay buffer	72 µL	Store plate in dark at RT
5	Baseline readout (FLIPR)	540 nm	Fluorescence readout 1 Hz for 1 min
6	Test compound	8 µL	10X compounds in assay buffer plate Incubation for 5 mins FLIPR readout 1 Hz
7	Stimulus	20 µL	5X stimulus buffer plate Incubation for 5 mins. FLIPR readout at 0.5 Hz.

Table 2. Steps for Na^+ influx screening assay campaign.

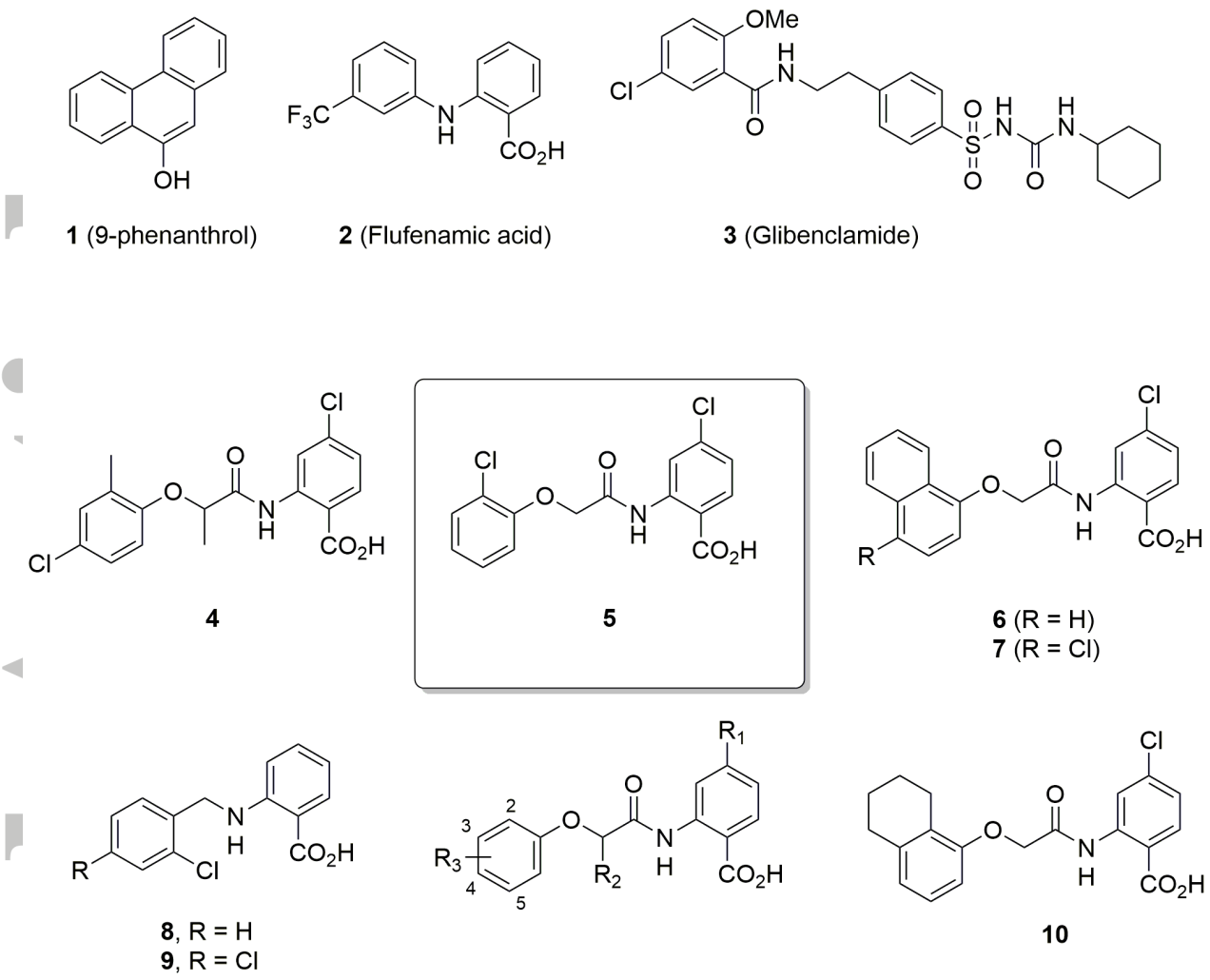

Figure 1. Chemical structures of TRPM4 inhibitors used in this study.

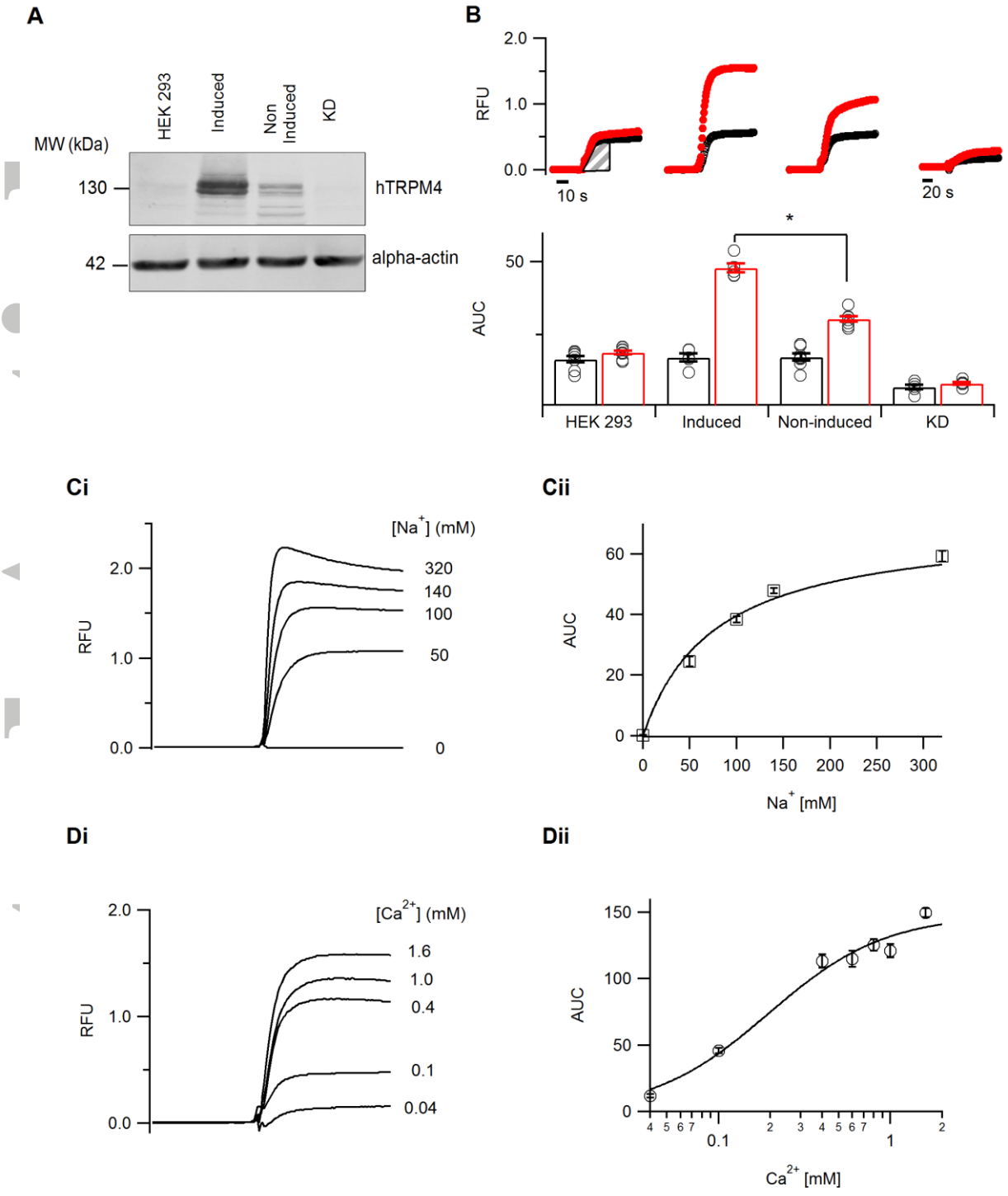

Figure 2. *Development and validation of a Na^+ influx screening assay:* **A)** Western blot analysis showing TRPM4 expression as detected by anti-TRPM4 antibody from whole-cell extracts prepared from HEK293 cells, TRPM4-expressing cells either induced with tetracycline or non-induced and TRPM4 CRISPR-Cas9 knocked-down cell line (KD). Alpha-actin served as a loading control. **B)** Averaged traces obtained on the FLIPR with Na^+-sensitive dye ANG-II in different cellular conditions as mentioned (panel A). The initial rate of fluorescence increase in either absence (black) or presence (red) of 10 µM ionomycin was deduced by measuring the area under the curve (AUC) from the shaded portion for different cellular conditions ($n \geq 5$). **Ci)** Averaged traces obtained on the FLIPR from TRPM4-expressing cells, with varying concentration of extracellular Na^+. **Cii)** The initial rate of fluorescence increase measured as AUC in different Na^+ concentrations were fitted using the

Michaelis-Menten equation ($n \geq 5$). **Di)** Averaged traces obtained on the FLIPR from TRPM4-expressing cells, with varying concentrations of extracellular Ca^{2+}. **Dii)** The initial rate of fluorescence increase measured as AUC in different Ca^{2+} concentrations were fitted using the Hill equation ($n = 6$). * $P \leq 0.05$, Student *t* test.

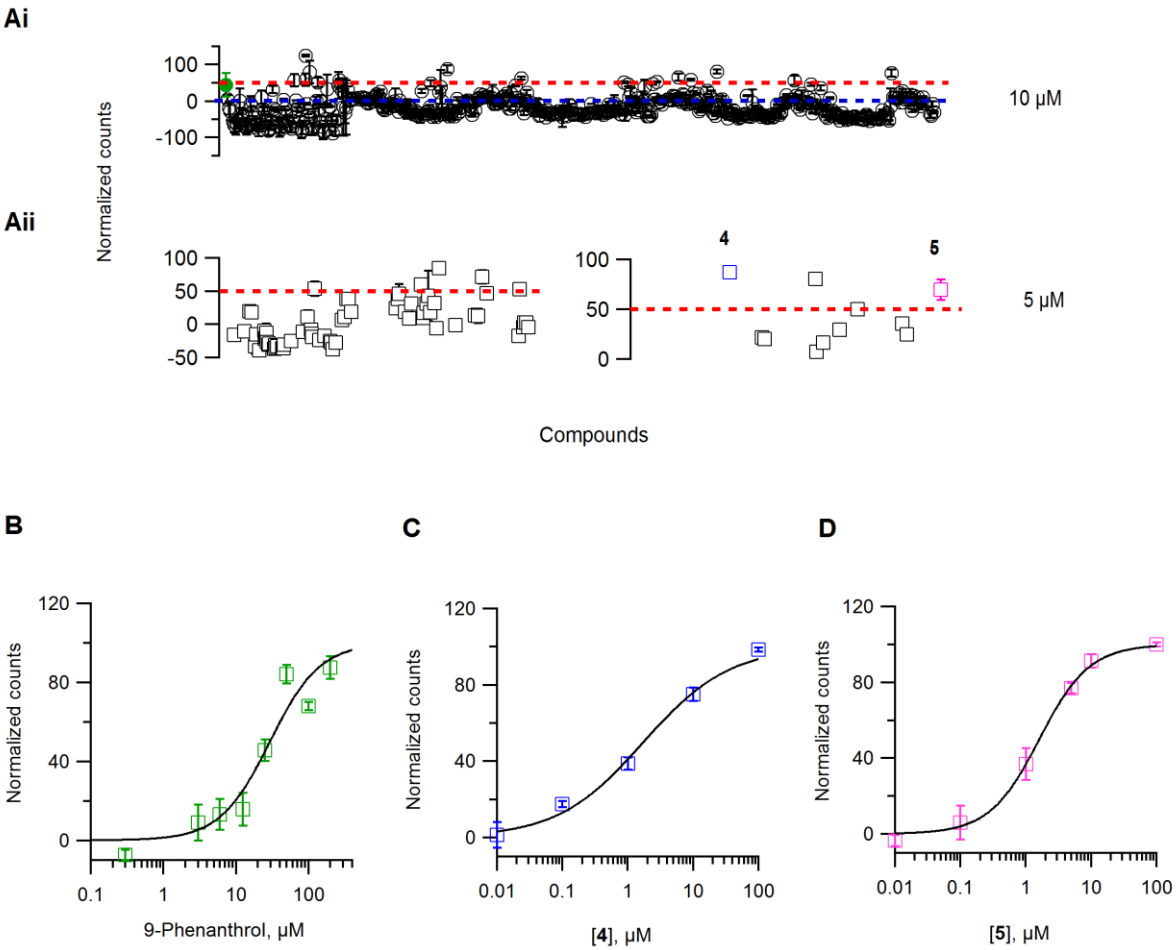

Figure 3. *Screening campaign for TRPM4 inhibitor* **Ai)** Representative scatter plot of normalized counts obtained from 470 compounds evaluated for inhibition of TRPM4-mediated Na^+ influx at 10 µM. Compounds above 0 (blue dotted line) were considered active **Aii)** Compounds with counts 50 or more (red dotted line) were retested twice at 5 µM. Each data point is averaged from two independent 96 well plates. (**B-D)** A concentration-response curve was constructed and the values were fitted with Hill equation to extrapolate IC_{50} values for 9-phenanthrol **(B)** and the newly identified inhibitors **4 (C)**, and **5 (D)** $n \geq 4$ for each concentration response curve.

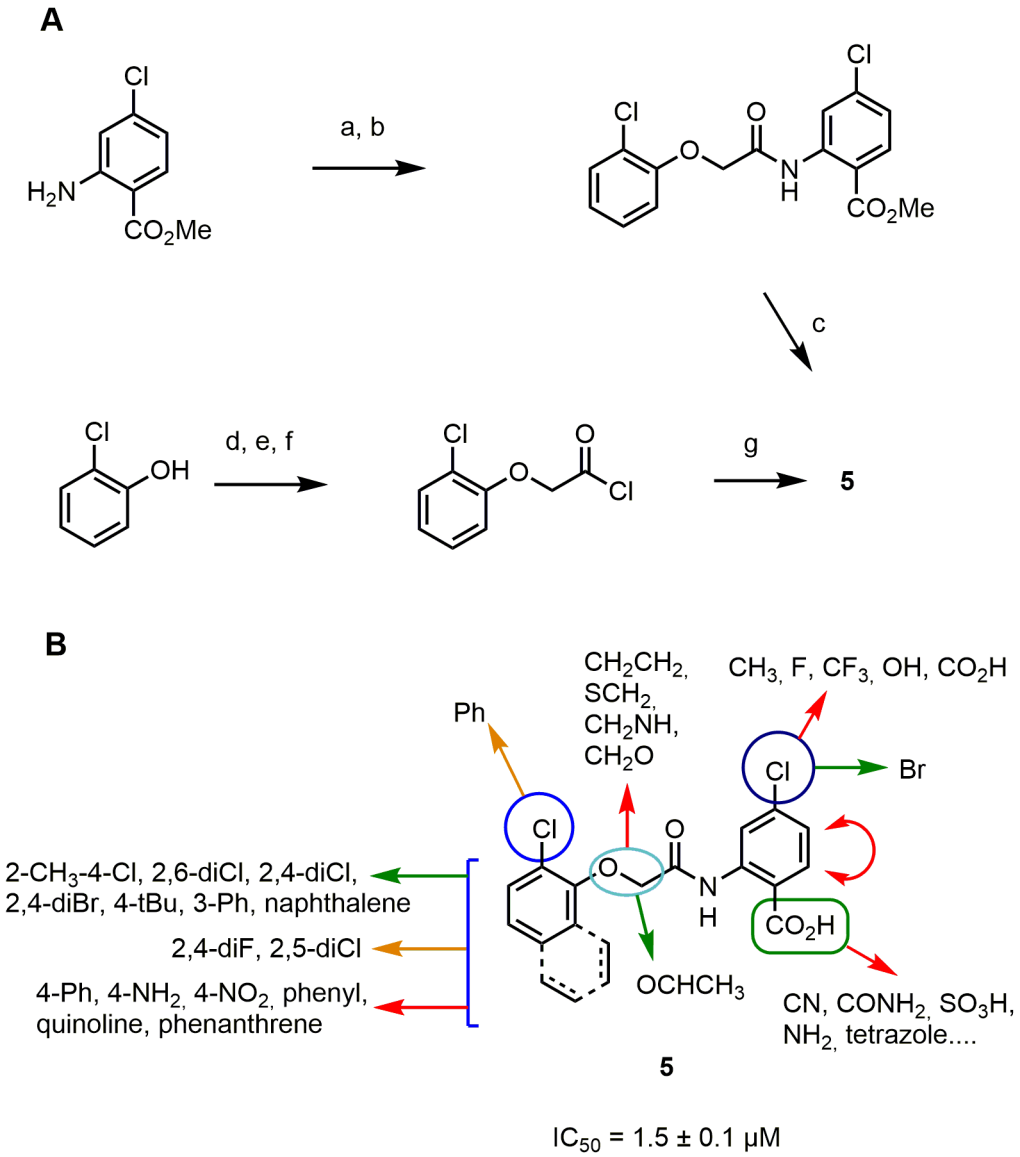

Figure 4. *Virtual screening guided discovery and optimization of TRPM4 inhibitors*. **A)**. Synthetic routes used to prepare compound **5** and analogs. Conditions: a) $ClCH_2COCl$, K_2CO_3, THF, room temperature (RT), 4h. b) 2-ClPhOH, K_2CO_3, DMF, 90°C, 2h30. c) KOH, MeOH/H_2O, reflux, 1h or LiOH, dioxane, RT, 1h. d) $ClCH_2COO$*t*-Bu, K_2CO_3, DMF, 80°C, 1h. e) TFA, RT, 1h. f) $SOCl_2$, DCM, reflux, 4h. g) 4-Cl-anthranilic acid, K_2CO_3, THF, RT, 2h. **B**) Overview of the structure-activity relationship uncovered by surveying 49 analogs. Green arrows indicate beneficial modifications and red arrows indicate deleterious ones.

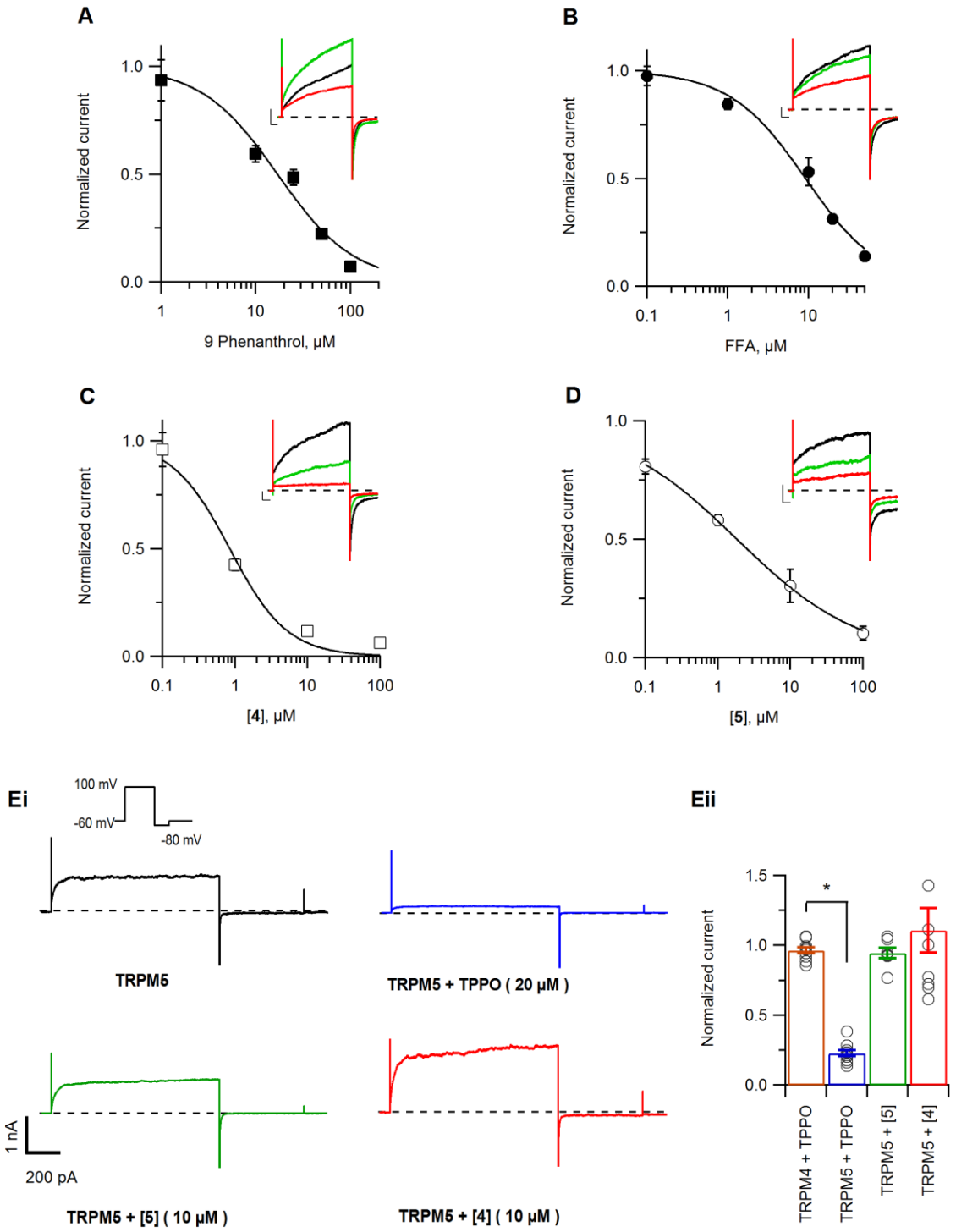

Figure 5. *Compound* **5** *is a potent and selective inhibitor of TRPM4 current.* TRPM4 currents were recorded from excised membrane patches exposed to 300 µM free Ca^{2+} on the cytosolic side of the patches. **A-D**) Concentration-response curves were obtained by applying various concentrations of 9-phenanthrol **(A),** FFA **(B)**, **4 (C)**, and **5 (D)**, dissolved in pipette solution. Currents were normalized to current without any inhibitor and fitted with the Hill equation to extrapolate IC_{50} values for each inhibitor. $n \geq 4$ for each concentration response curve. Representative current traces were overlapped at 0 µM (Black), 1 µM (Green) and 10 µM (Red) concentration of the inhibitor (Scaling: X-axis 50 ms, Y- axis 500 pA). **E**) Selectivity of compounds **4** and **5** mediated inhibition of TRPM5 currents recorded using a voltage-step protocol (figure inset) from HEK293 transiently transfected with

TRPM5. **Ei)** Representative trace of TRPM5 current from excised membrane patches exposed to 50 µM free Ca^{2+} on the cytosolic side of the patches either inhibited by TPPO (blue), **5** (green), or **4** (red). **(Eii)** Average currents measured at +100 mV were normalized to current without any inhibitor ($n \geq 8$). * $P \leq 0.05$, Student *t* test.

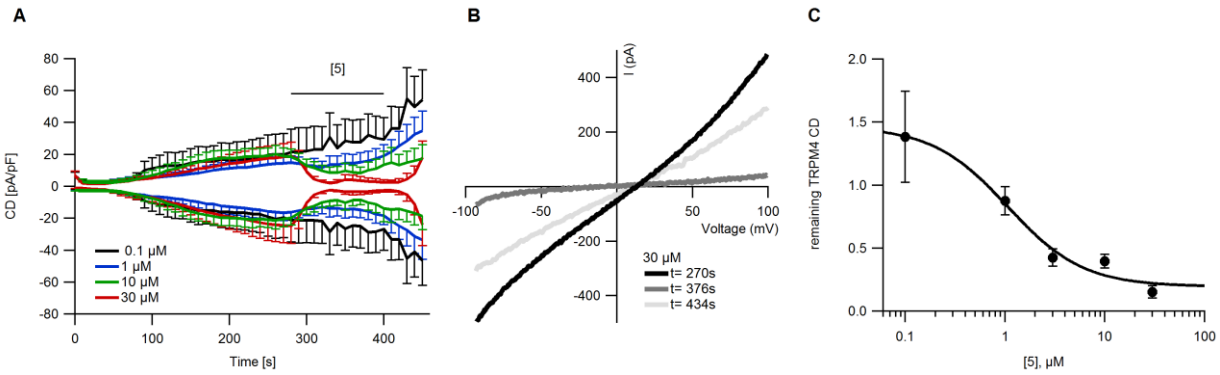

Figure 6: *Compound* **5** *reversibly blocks endogenous TRPM4 currents in LNCaP prostate cancer cells* **A)** Time course of average TRPM4 current densities (CD) activated in LNCaP cells by intracellular Ca^{2+} when various concentrations of **5** were applied. n = 5 (0.1 and 1 µM), 6 (10 µM) and 3 (30 µM). **B)** Exemplary I-Vs from cells in (A) when TRPM4 current was developed (t = 270 s) and blocked with 30 µM compound **5** (t = 376 s) and washout (t = 434s). **C)** Dose-response curve for TRPM4 currents when different concentrations of **5** were applied (same cells as in A). CD at 376 s was normalized to CD at 270 s and plotted versus concentration of **5**. $n \geq 3$ for each concentration of **5** . Data were fitted with a Hill equation to extrapolate the IC_{50}.

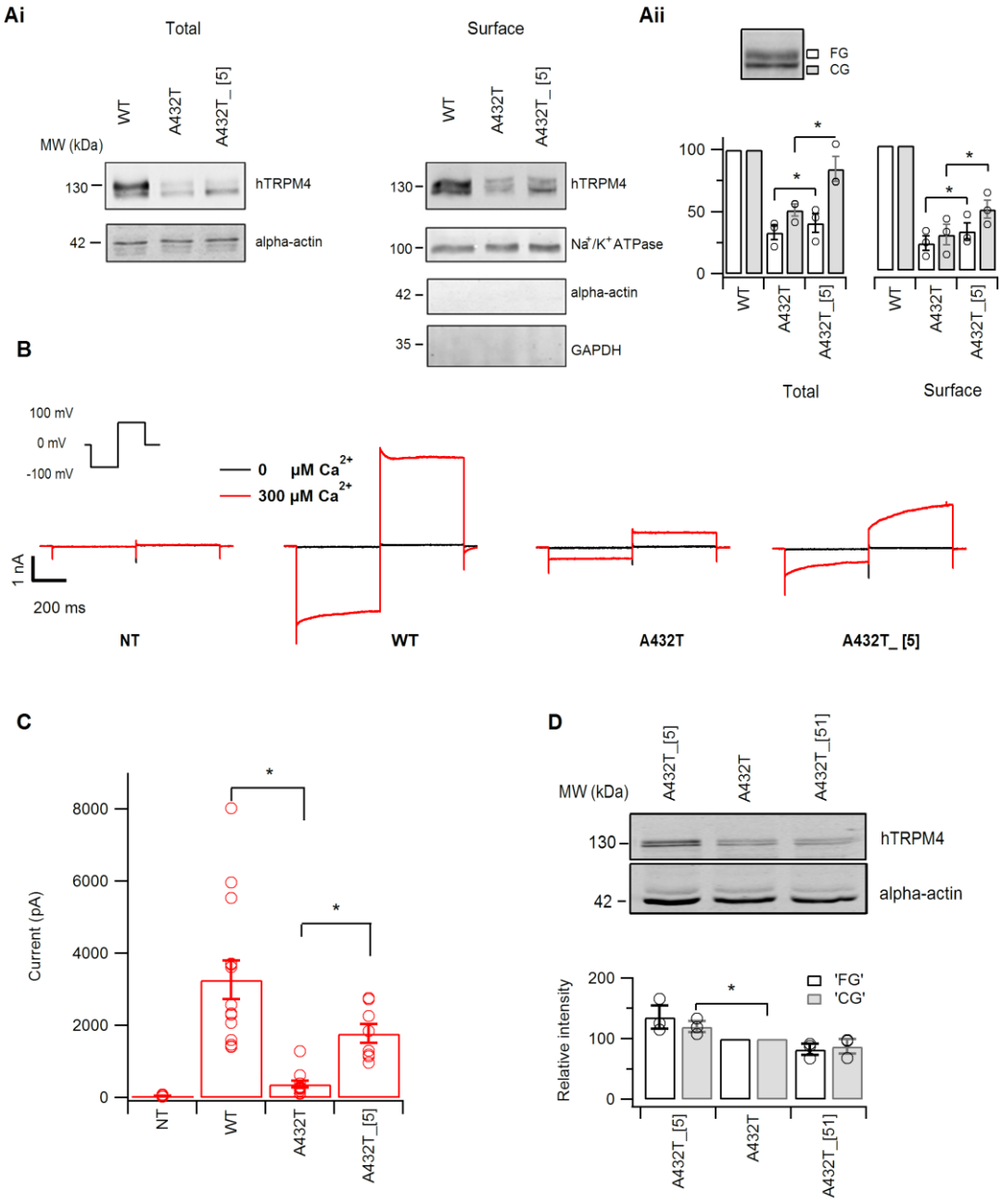

Figure 7: *Functional assessment of A432T variant rescue by compound* **5**. **Ai)**Western blot analysis show rescue of A432T variant total and surface expression by 50 µM compound **5**, as detected by anti-TRPM4 antibody. **Aii)** Densitometry quantification of blots at total and surface level expression show compound **5** rescued both the core and fully glycosylated form of A432T. The protein band intensity at each concentration was quantified from 3 individual experiments. **B)** Representative inside-out voltage clamp recordings on membrane patches from non-transfected (NT) or heterologously expressing TRPM4 WT, A432T, or A432T pre-incubated with 50 µM compound **5** (A432T_**[5]**), when exposed to nominally either 0 or 300 µM Ca^{2+} on the cytosolic side. **C)** Average current amplitude measured at the end of voltage step to + 100 mV (inset, panel B) ($n \geq 5$). **D)** Western blot analysis showing membrane expression rescue of A432T variant by active compound **5** and not by inactive congener **51** at 50 µM ($n = 3$)**.**

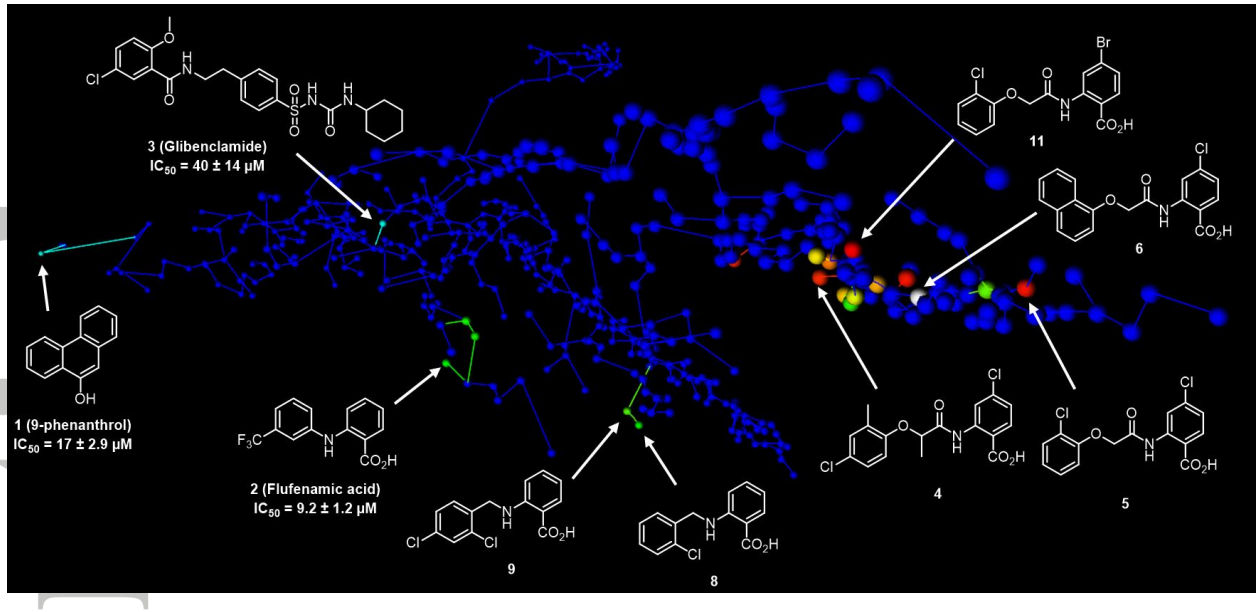

Figure 8. *Chemical space analysis*. Selected view of an interactive 3D-map of substructure fingerprint similarity representing each of the 470 compounds tested as one sphere. The map is color-coded by pIC_{50} value from blue (lowest value) to red (highest value). The interactive map is accessible at http://gdbtools.unibe.ch:8080/webMolCS/yourSIM.html?jobID=1506356578836&fp=Sfp.